energies

MDPI

Article

Thermochemical Conversion of Biomass in the Presence of Molten Alkali-Metal Carbonates under Reducing Environments of N_2 and CO_2

Tahereh Jalalabadi, Behdad Moghtaderi and Jessica Allen *

School of Chemical Engineering, University of Newcastle, Callaghan, NSW 2308, Australia; tahereh.jalalabadi@uon.edu.au (T.J.); Behdad.Moghtaderi@newcastle.edu.au (B.M.)

* Correspondence: j.allen@newcastle.edu.au; Tel.: +612-40-339-359

Received: 15 September 2020; Accepted: 12 October 2020; Published: 15 October 2020

Abstract: The impact of N_2 and CO_2 atmospheres on the interaction between Eucalyptus pilularis biomass and a ternary molten carbonate eutectic (Li_2CO_3: Na_2CO_3: K_2CO_3) has been investigated at 600 °C and 900 °C. For lower temperature conversion under CO_2, prevention of volatile release in the eutectic treated biomass is slightly higher than under N_2 injection; however, similar bubble-shaped morphology of the remnant char is observed under both carrier gases. By increasing the temperature to 900 °C under CO_2, the reverse Boudouard reaction begins to consume carbon fuel, while molten carbonate gasification also accelerates the reaction to a lower temperature set point (shifted from ~735 °C to ~640 °C). The mass loss of carbonate under CO_2 and N_2 at 900 °C is 0 (negligible) and 18 wt.%, respectively. In the absence of carbon particles, the decomposition of carbonate to M_2O (l) and CO_2 (g), as well as molten salt vaporization, are the sole potential routes of weight loss in an inert gas. Previous observations of biomass and eutectic mixture thermochemical conversion under N_2 have suggested carbon/carbonate gasification is dominant at elevated temperatures, with production of CO expected. However, analysis of gas chromatography (GC) suggests that carbon/carbonate gasification is the weaker pathway by producing only 7 vol.% of CO, compared with molten carbonate decomposition with 27 vol.% CO_2 emission for this system.

Keywords: slow pyrolysis; Boudouard reaction; carbonate gasification; ternary eutectic; biomass

1. Introduction

Thermochemical conversion is considered the most ancient procedure in biomass utilization. The reaction pathway categorized is based on temperature and oxidizing agent. From this perspective, pyrolysis takes place in the absence of oxygen (often under N_2 or Ar environments), combustion takes place in a full oxidizing environment (typically air with excess oxygen), and gasification is carried out under a partial oxidizing environment (often mixtures of air with CO_2 or steam) [1]. For decades, researchers have investigated the benefits of biomass gasification and pyrolysis in comparison with a more tradition pathway of combustion [2–7].

Pyrolysis of biomass heavily depends on heating rate (classified between slow and fast) [8,9], which produces biogas (mainly, CO, CO_2, H_2, and CH_4), bio-oil (brown greasy mixture of non-condensable volatiles), and bio char (solid carbonaceous residue) [10–12]. During pyrolysis of biomass, each inherent component of feedstock (such as hemicellulose, cellulose, and lignin) decomposes through its own individual pathway at different operational temperature ranges (from ~200 °C for hemicellulose to approximately 600 °C for lignin) [13,14]. In contrast with pyrolysis in an inert gaseous environment, endothermic and heterogeneous gasification of biomass under steam and CO_2 provides well known paths of steam gasification (reaction-4) [15] and Boudouard conversion (reaction-5) [7] with production of CO and H_2. Key reactions in biomass gasification are listed in Table 1.

Table 1. Oxidation and gasification reactions in biomass thermal conversion [1].

Number	Reaction	ΔH^{o}_{R}
	Oxidation Reactions	
1	$C + \frac{1}{2} O_2 \rightarrow CO$	−111 (MJ/kmol)
2	$CO + \frac{1}{2} O_2 \rightarrow CO_2$	−283 (MJ/kmol)
3	$H_2 + \frac{1}{2} O_2 \rightarrow H_2O$	−242 (MJ/kmol)
	Gasification Reactions	
4	$C + H_2O \rightarrow CO + H_2$ (Water-Gas reaction)	+131 (MJ/kmol)
5	$C + CO_2 \rightarrow 2CO$ (Boudouard reaction)	+172 (MJ/kmol)
6	$C + 2H_2 \rightarrow CH_4$ (Methanation reaction)	−75 (MJ/kmol)
7	$CO + H_2O \rightarrow CO_2 + H_2$ (Water–Gas–Shift reaction)	−41 (MJ/kmol)
8	$CH_4 + H_2O \rightarrow CO + 3H_2$ (Methane–Steam reforming)	+206 (MJ/kmol)

CO_2 gasification is thermodynamically favored at temperatures above 680 °C (a similar temperature to steam gasification [16]). The environmentally friendly route of CO_2 consumption, through solitary CO production via Boudouard reaction, counts as an advantage for commercial scaled-up CO_2 gasification plants compared with steam gasification [11]. To understand pyrolysis and CO_2 gasification routes of biomass, different groups have investigated the effect of variables, such as the nature of feedstock [7,17,18], the catalytic role of chemical additives, such as alkaline metal salts [19–24], hydroxides [25,26], chlorides [27,28], and the heating rate to the final working temperature [9,22,24,29,30]. However, during pyrolysis up to 680 °C (known gasification starting temperature), the major reaction regime is devolatilization and primary char production, while gasification is an extension of pyrolysis at a higher temperature when conducted with carbon dioxide (>~680 °C) [12]. Although there are a significant number of reports in addressing biochar modification under CO_2 and N_2 [29–31], this has mainly been done in the absence of chemical additives. For example, in a recent work, Kim et al. [31] reported char modification resulting from different types of feedstock (such as cellulose, lignin, xylan, grass, and oak wood) during both slow and fast heating rates up to 680 °C, avoiding Boudouard gasification (reaction-5). Based on their findings, carrier gas impact on remnant char surface area is highly dependent on input feedstock, and the notable improvement of BET_{sur} results demonstrated large variation in outcomes of oak wood (231.15 m^2g^{-1} under N_2 and 463.58 m^2g^{-1} under CO_2) with less impact on cellulose (507.53 m^2g^{-1} under N_2 and 506.94 m^2g^{-1} under CO_2). Senneca's group [29] also acknowledged the impact of a gaseous atmosphere on walnut shell thermochemical conversion with ramping rate (5 to 20 °C/min) up to 900 °C, the outcome being a higher amount of O/C and H/C for char prepared under N_2 compared to CO_2, which makes it more reactive in combustion.

However, the impact of carrier gas while using chemical additives, such as alkaline carbonates, during biomass conversion is not well understood. The high thermal expected stability of molten carbonate and its catalytic influence on the Boudouard gasification reaction attracts many researchers to broadly explore biomass gasification modified by this additive [3,23,32,33].

However, the decomposition of carbonate salts (reaction-9, where M represents alkali-metals Li, Na, or K) is suggested by other researchers, particularly above 700 °C [34–39].

$$M_2CO_3 \rightarrow M_2O + CO_2 \ (\text{Reaction} - 9)$$

It is observed that molten carbonate displays negligible mass loss under CO_2 compared with inert gas (Ar, N_2) and air injection. Alongside molten carbonate chemical decomposition, some studies have also suggested vaporization of carbonate at high temperatures [19,22,40].

In the presence of carbon fuel, there is an additional route of carbonate consumption under N_2, which is the result of its reaction with carbon particles. Above 700 °C, reaction-10 takes place to generate M_2O and CO, which is known as carbon/carbonate gasification [34,41] or carbothermal reduction [39].

$$M_2CO_3 + C \rightarrow M_2O + 2CO \,(\text{Reaction} - 10)$$

In a carefully designed study, Kopyscincki et al. [22] investigated the gaseous output of this reaction with major emission of CO from reaction-10 for acid washed coal conversion after addition of K_2CO_3 under both CO_2 and N_2 up to 800 °C.

To lower the melting point of alkali-metal carbonate additives, combining salts with different ratios is favored, specifically in high temperature fuel cell technology [42–44]. Exploration of binary compositions of carbonate [40,45] or ternary eutectic [46–49] with lower melting points have been used extensively. Currently, there is a lack of precise information on a ternary molten carbonate interaction with carbon materials, such as biomass, under N_2 and CO_2, and separating the influence of potential reaction pathways has not been achieved to date.

The objective of this work is to explore the impact of injected gas (N_2 vs. CO_2) on thermochemical conversion of woody biomass mixed with molten carbonate ($[LiNaK]_2(CO_3)$) with a slow heating rate (5 °C/min) from ambient temperatures to two different higher heating temperatures (HHT at 600 °C and 900 °C). The weight losses of all treated and untreated samples were recorded by thermogravimetric analysis (TGA) and by measuring the amounts of CO and CO_2 emission with inline gas chromatography (GC).

2. Materials and Methodology

The Eucalyptus Pilularis woody biomass of our previous study [19] with average particle size range (75–150 μm) was applied in this work and the ternary eutectic contained a mole percentage mixture of Li_2CO_3:43.5%, Na_2CO_3: 31.5%, and K_2CO_3: 25% with a melting point (~400 °C). This particle size range provided good particle contact between salts and biomass prior to salt reaching the molten state. All samples were dried in the oven (110 °C) overnight and mixed with a 50 wt.% impregnation ratio. For each experiment, 50 mg of dried sample was loaded in an alumina crucible with a platinum handle (inner diameter: 15 mm; height: 10 mm) and placed inside a Rubotherm high pressure TGA (HP-TGA). Both gasification and pyrolysis were run with a heating rate of 5 °C/min under 100 mL/min of selected gases, followed by 120 min of isothermal treatment at two HHT (600 °C and 900 °C). For lower deviation of results, each experiment was repeated three times with a standard error recorded. For biomass thermochemical conversion tests at 900 °C, gas analysis of CO and CO_2 emission was measured, where the Rubotherm HP-TGA outlet was connected to an Agilent 490 micro gas chromatograph (GC), which contains two columns and two thermal conductivity detectors (TCDs).

Additionally, after washing samples with hot distilled water (80 °C, details explained in [19]), the morphology of prepared chars from different types of injection was carried out via scanning electron microscopy (SEM) on a Ziess Sigma VP FESEM.

For further experiments, the char of biomass was produced in a horizontal tube furnace CHY-1200 (Model: T1250S) under N_2 (100 mL/min) via slow pyrolysis (5 °C/min) to 600 °C and 2 h isothermal condition before cooling to an ambient temperature.

Naming conventions for a sample references its input condition to the test as raw biomass (Bio) or biomass char (Char), treated or untreated by carbonate (Bio indicates untreated and Bio50 expresses mixture with 50 wt.% of eutectic, as does Char50), and whether the test was completed under N_2 or CO_2 (Bio50-N_2, Bio50-CO_2, Char50-N_2 and Char50-CO_2).

3. Results

3.1. Thermochemical Conversion under N_2 vs. CO_2 at Low HHT (600 °C)

The primary results of biomass conversion under N_2 and CO_2 at 600 °C are illustrated in Figure 1. As there are no changes during 2 h isothermal tests at 600 °C, only 15 min of isothermal results are presented, with an initial temperature above 200 °C. Mass loss change versus time for untreated biomass (Bio) under N_2 and CO_2 show narrow deviation with only slight further devolatilization above 350 °C under CO_2 compared to N_2 (Figure 1A). This is in agreement with previous findings for modification of biomass char under CO_2 without any additives [29,31], with low overall impact on solid and liquid products, in contrast with effects reported about coal [50].

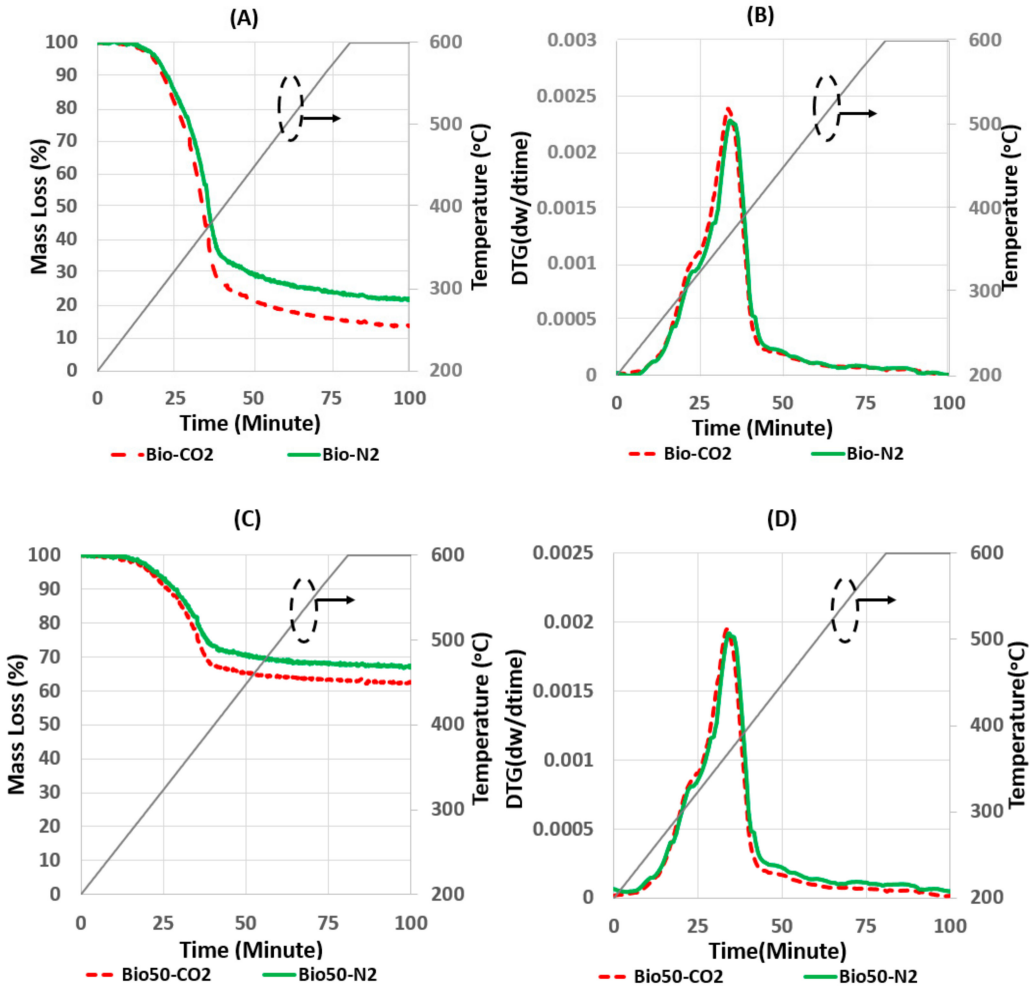

Figure 1. Thermogravimetric analysis (TGA) mass changes (**A**,**C**), and DTG curves (**B**,**D**) of Bio and Bio50. Conversion under N_2 and CO_2 at 600 °C.

Observation from differential thermogravimetric DTG curves of Bio pyrolysis and gasification in Figure 1B presents minor discrepancy, peak shifts, and peak height changes.

In the case of Bio50, the same outcome with a minor effect of injected gas on volatile removal is recorded, while lower total amount of mass loss (wt.%) in Bio50-N_2 and Bio50-CO_2 is expected due to the addition of thermally stable salt. $[LiNaK]_2(CO_3)$ has an inhibitive impact on biogas emission from both Bio50-N_2 and Bio50-CO_2, which is in agreement with our previous works [19,48]. In untreated Bio-CO_2, total mass loss was recorded at 86 wt.%, and after modifying mass loss of Bio50-CO_2 (excluding weight of carbonate) devolatilization of the treated sample was 6 wt.% different with only

80 wt.% lost. Molten carbonate is fairly stable at 600 °C under both N_2 and CO_2 with minor weight loss (less than 2 wt.%), but above 400 °C (when it transforms to liquid phase), the additive has still been shown to influence the biomass devolatilization mechanism, generating bubble-shaped carbonaceous particles and a porous structure of woody biomass [19].

Previous works [39,48] suggest no interaction between carbonate and carbon at 600 °C, which means carbonate gasification reaction will not take place at this temperature. In regard to this, the stability of carbonate and carbon/carbonate gasification is examined by investigating Char50 and the pure eutectic under both pyrolysis (N_2) and gasification (CO_2) conditions in Figure 2.

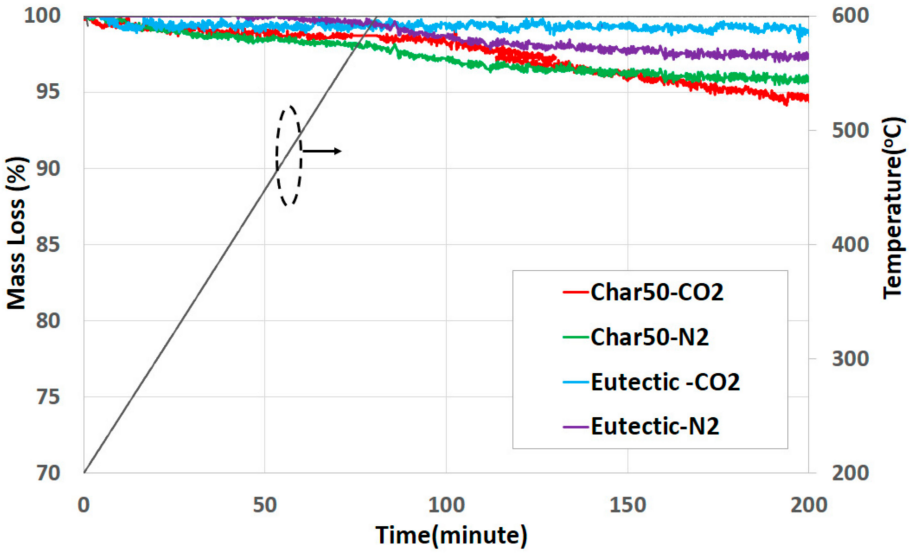

Figure 2. TGA mass changes Char50 decomposition and eutectic stability under N_2 and CO_2 at 600 °C.

Figure 2 presents the mass loss of eutectic up to 600 °C under N_2 (approximately 2 wt.%) and 0% (negligible) under CO_2, and both Char50-CO_2 and Char50-N_2 show less than 5 wt.% mass loss to the end of isothermal test time (2 h). This outcome relates to plausible removal of any remaining volatiles in the prepared char and slight decomposition of molten carbonate.

To understand morphology of remnant char from Bio50-CO_2, water washed sample (Section 2) SEM images are expressed in Figures 3 and 4. The overall view, with 100x magnification image in Figure 3, clearly recorded agglomerated particles with some ruptured shapes (highlighted with a yellow circle), which is in accordance with Bio50-N_2 morphology (detailed images are available in [19] and SEM images of N_2 are in supplementary data Figure S1). In Figure 4, by exploring more particles (A and E are two different particles) and higher magnification (B–D, F–H), the swollen particles and bubble structure were extensively sighted, along with some remaining salt residue (needle shape white minerals). This similarity of results confirmed the minor mass loss deviation of Bio50 conversion under N_2 and CO_2 from TGA analysis (Figure 1). The effect of swelling in carbon particles was also clearly observable, which was stated by other groups, mostly during the softening stage of coal [51,52] or biomass [53,54] in different thermochemical conversion pathways. The presence of molten carbonate, specifically above its melting point (600 °C), modifies condensable and non-condensable volatile emission and manipulates char structures. Previous observation of tar reduction and volatile evolution changes for treated biomass was carried out in an inert environment (N_2) of pyrolysis [19,48]; however, here, it is confirmed that this also occurs under CO_2 with molten carbonate treatment up to 600 °C. It can be concluded that molten carbonates impact on volatile release is independent of gaseous surroundings at working temperatures less than gasification (reaction-10) and vaporization.

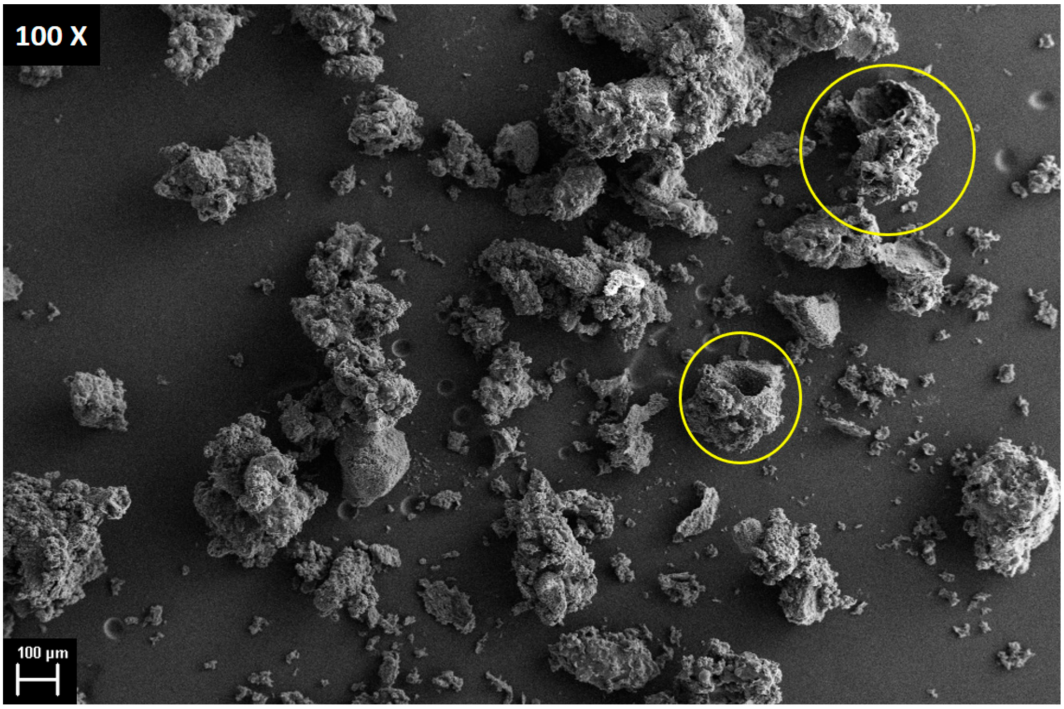

Figure 3. SEM image of particle distribution of washed Char from gasification of Bio50 at 600 °C.

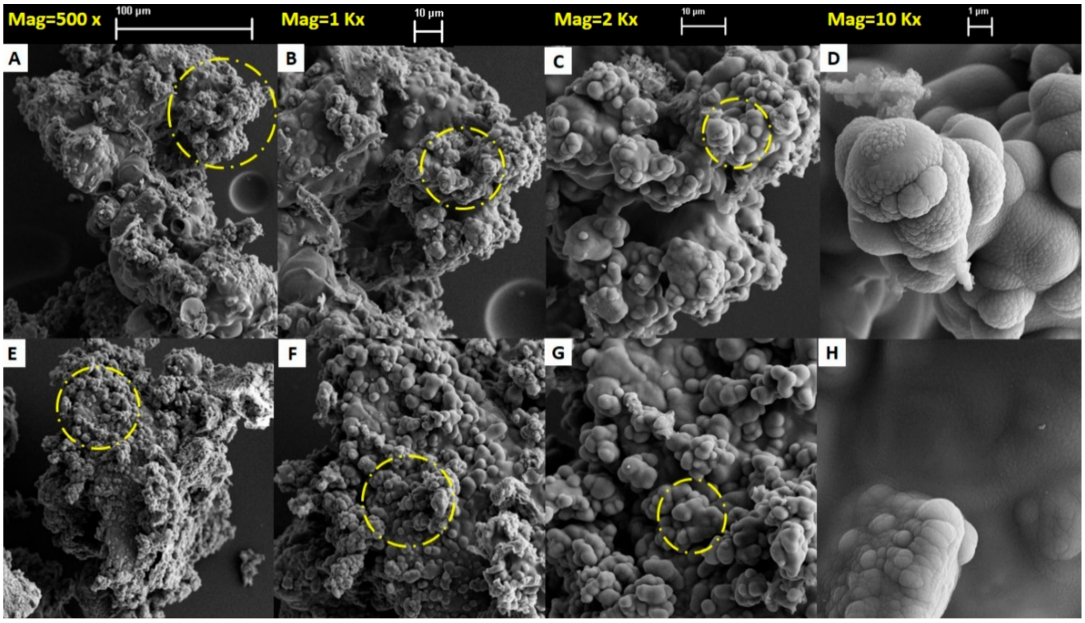

Figure 4. SEM image of particle distribution and surface morphology from Bio50-CO_2 water washed at 600 °C (**A**–**D**) Example particle at increasing magnification (**E**–**H**) additional particle at increasing magnification.

3.2. Thermochemical Conversion under N_2 vs. CO_2 at High HHT (900 °C)

By increasing the temperature to 900 °C, the plots of mass loss versus temperature (°C) are shown in Figures 5 and 6, where samples underwent drastic changes in mass. Initial results of biomass pyrolysis and gasification in Figure 5A,C,D displayed a similar trend to previous results from 600 °C (Figure 1) and, again, a slightly higher amount of mass loss under CO_2. Under N_2, biomass devolatilization was fully accomplished approximately at 600 °C and no further mass loss was expected at the elevated temperature. However, under CO_2 and above ~750 °C, there was a second

weight decrease and peak of the DTG curve (Figure 5C,D), potentially resulting from Boudouard gasification (reaction 5). In the case of biomass gasification, the set point of the Boudouard reaction was recorded at ~735 °C, which can be seen in derivative curves based on temperature in graph C and time in graph D of Figure 5.

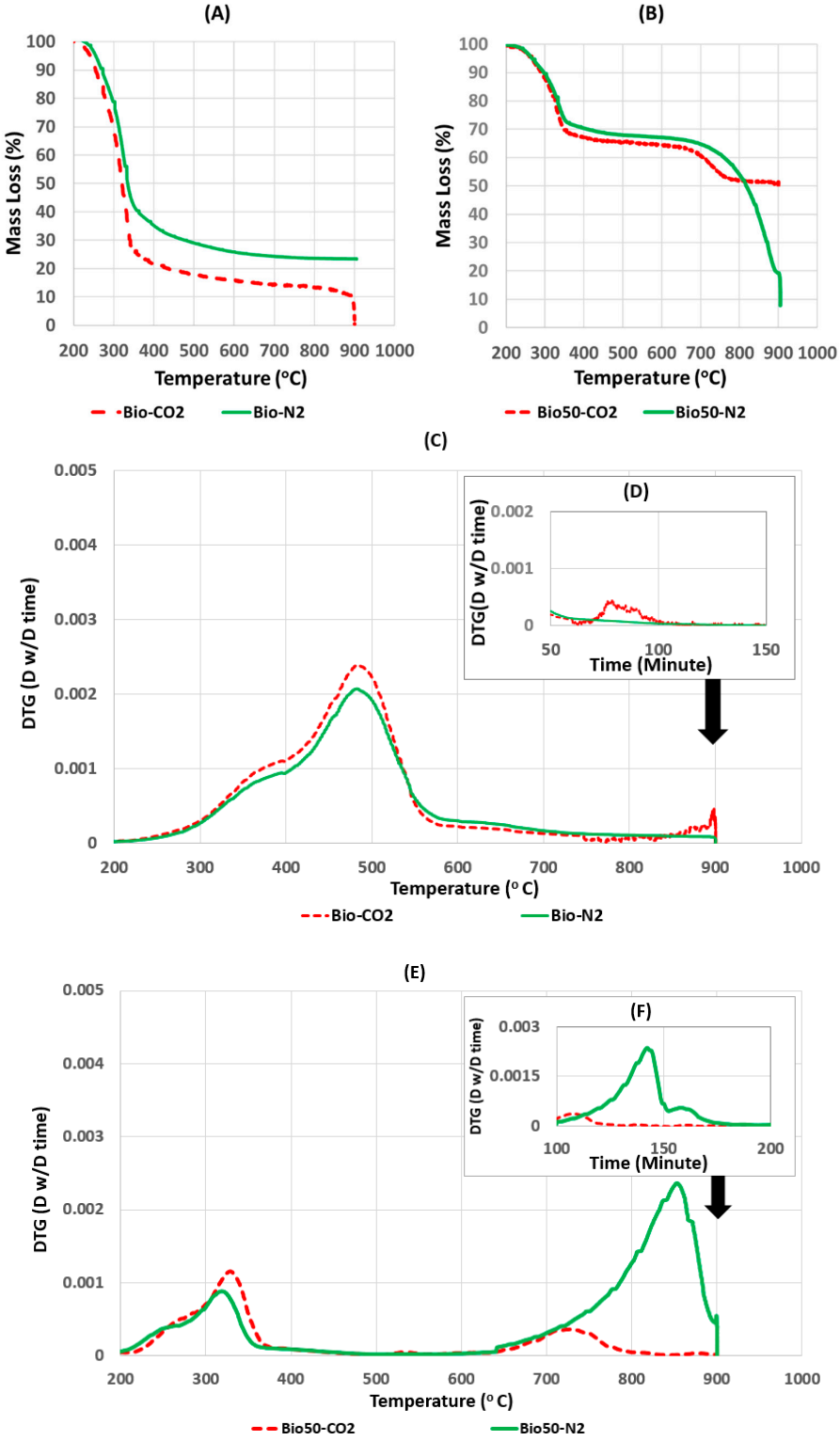

Figure 5. TGA mass changes (**A**,**B**) and DTG curves (**C**–**F**) of Bio and Bio50 thermochemical conversion under N_2 and CO_2 at 900 °C.

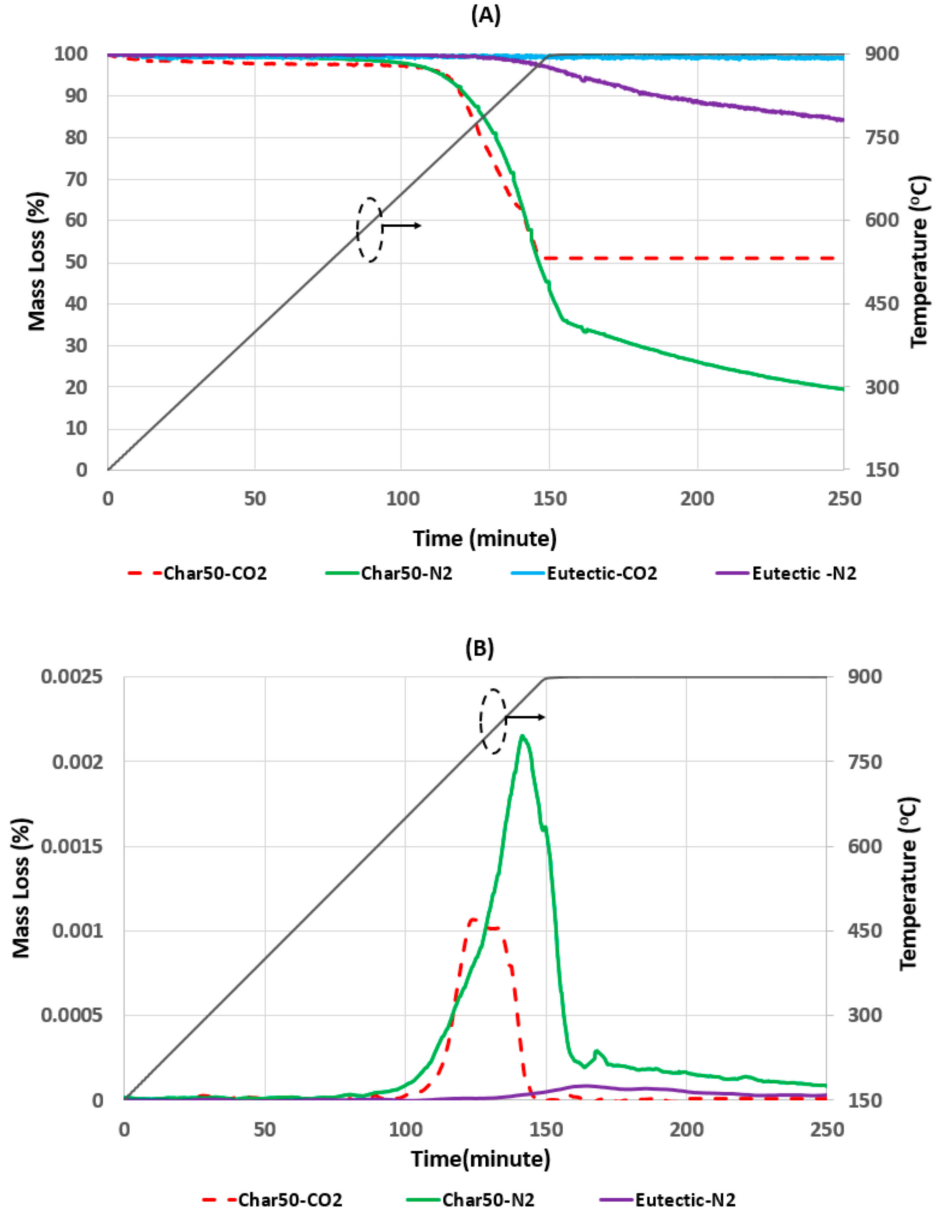

Figure 6. TGA mass changes (**A**) and DTG curve (**B**) of Char50 and eutectic. Stability under N_2 and CO_2 at 900 °C.

For the next step, comparison of Bio50-N_2 and Bio50-CO_2 was investigated (Figure 5B,E,F), and for both conversion procedures, the impact of molten carbonate was profound.

In Figure 5B, presumably by passing the devolatilization stage (<600 °C), we already had a mixture of solid char and molten carbonate in the system. Thus, a weight loss of Bio50-N_2 above 750 °C (green line) is an indication of carbon/carbonate interaction (reaction-10) and molten carbonate decomposition (reaction-9), as well as possible vaporization. The starting point of this change was recorded at 660 °C and continued during 2 h isothermal at 900 °C.

On the other hand, in Bio50-CO_2, eutectic is expected to be firmly unreactive (no mass loss originates from salts from either decomposition of vaporization, according to results in Figure 6) and Boudouard gasification is the expected reason for TGA mass loss or DTG peaks (Figure 5B,E,F). It is believed that carbonate decomposition (reaction-9) is thermodynamically less likely in this case; however, carbon/carbonate gasification (reaction-10) might be plausible, as well as dominant Boudouard gasification (reaction-5), where CO becomes the favored product. As it has been shown in

the literature, alkali-metal carbonates catalyze the Boudouard reaction [11,24,55,56], thus, there was a backshift in DTG by a primary onset at 640 °C, which implied accelerated reaction-5 in comparison with untreated Bio (onset at ~735 °C). Figure 5E,F enables us to distinguish peak differences of both Bio-CO_2 and Bio-N_2. As it is explained, in the case of CO_2, there was an individual pathway of carbon gasification (reaction-5) that generated a single peak (red dashed in Figure 5E,F). This peak was smaller than the Bio-N_2 mass loss, which was related to the amount of sample at 600 °C. All tests started with biomass (not biochar), which, during devolatilization, lost almost 75 wt.% of its primary weight. Thus, by reaching to 700 °C, only a small amount of carbon remained in the eutectic to react with CO_2. This was in contrast with Bio50-N_2, which would be expected to contain a similar amount of char, but follows a more complex mass loss from the transformation of both media still present (carbon and molten salts).

To elaborate on this phenomena, the reactivity of prepared and carbonate mixed char (preparation procedure explained in Section 2) under CO_2 and N_2 (named Char50-CO_2 and Char50-N_2) was examined, as well as the stability of $[LiNaK]_2$ (CO_3) up to 900 °C (Figure 6). As expected, eutectic stability under CO_2 showed no mass loss, in contrast with almost 18 wt.% degradation under N_2, in line with our previous outcome for N_2 gas atmospheres [19]. Vaporization of carbonate in this case was only observed to cause the TGA crucible to stick to the walls, suggesting vaporization and fusion of carbonate within the analysis equipment (as pictured in Figure S2 in supplementary data). This time, by loading the same amount of stabilized carbon-rich char for both treated pyrolysis and gasification, Char50-CO_2 demonstrated almost 47 wt.% mass loss (from 640 °C to 880 °C), and the DTG peak height could be seen to be higher than Bio50-CO_2 (Figure 5E,F). Additionally, a decrease of weight continued for Char50-N_2 to the end of the 2 h isothermal period (900 °C), in line with results of decomposition (reaction-9) and vaporization expected to occur for the pure eutectic. According to plotted data in Figures 5F and 6A,B, there were two steps of mass loss and two peaks in Bio50-N_2 and Char50-N_2. It was be expected that the first peak (before reaching 900 °C) might originate from carbon/carbonate gasification, since this mass loss was not observed for the pure eutectic. However, in the presence of carbon particles, carbonate decomposition and vaporization must have also occurred, since the mass loss in this section exceeded the mass of carbon present (>50 wt.%) and continued further into the isothermal period. The mass loss of Char50-N_2 represented a two-step mass loss, as shown in Figure 6A. It is suggested here that the major mass loss first experienced by the mixture was mostly a result of carbon catalyzed carbonate decomposition and vaporization. When the temperature stabilized the remaining carbonate particles, the carbon could then undergo further carbon/carbonate gasification (recation-4). To understand this, GC analysis of Bio50-N_2 and Bio50-CO_2 is interpreted in Figure 7.

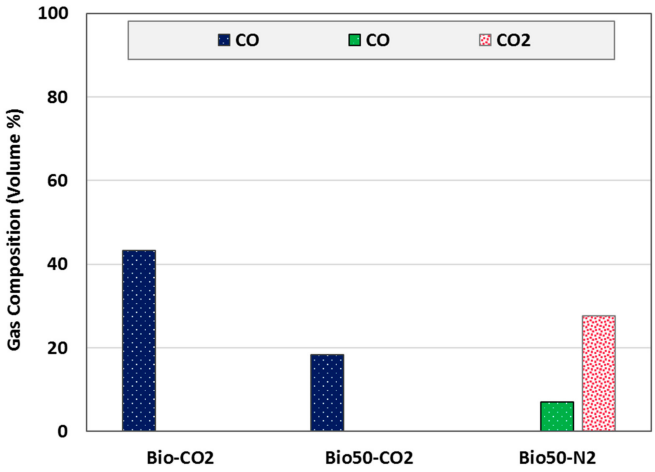

Figure 7. Volume % of emitted CO and CO_2 from different samples conversion under N_2 and CO_2 above ~600 °C.

The amount of CO generated from Bio-CO_2 appeared to be more than Bio50-CO_2 (~24 vol.% difference), which is regarded a result of a lower amount of applied carbon in the treated sample.

Carbon/carbonate gasification took place under N_2 and results in ~7 vol.% of the gaseous outlet CO. Production of ~27 vol.% CO_2 from Bio50-N_2 supported the sharp peak of DTG and expressed a mass loss of TGA in Figures 5 and 6, seemingly as a circumstances of strong, likely carbon-enhanced carbonate decomposition (reaction-9). This is in agreement with previous intuition from McKee and Chatteriji [57], who investigated graphite conversion (treated with Na_2CO_3 at 600 °C) in low CO_2 environment, where results indicated enhanced carbonate decomposition. Peng et al. [44] applied post-test Energy Dispersive X-Ray Analysis EDX analysis and detected a higher amount of metal oxide formation under N_2 carbothermal reduction of coal from Li-K carbonate compared with CO_2 (from 650 to 750 °C). Physical vaporization of carbonate at this temperature is another plausible pathway that we witnessed during our experiments at 900 °C, but is difficult to quantify (Figure S2, supplementary data). Additionally, as the major component of gaseous outlet was CO_2 rather than CO, it could be seen that the premier mass loss, as shown in Figure 5E,F and Figure 6B, of treated samples must relate to decomposition rather than gasification, which would result in much higher CO formation. Thus, the intricate mechanism of carbonate under N_2 and in presence of carbon, underwent different steps from physical changes of salt (vaporization) to known and unknown extent of chemical reactions (such as decomposition and gasification), while in a CO_2-rich atmosphere, Boudouard consumption (reaction-5) was catalyzed in the presence of otherwise stable and unreactive $[LiNaK]_2(CO_3)$.

4. Discussion

According to the described results in Section 3, it is essential to elaborate internal phenomena during treated biomass pyrolysis and gasification at a high temperature (~900 °C). As it is shown in graphical illustration in Figure 8, the right side represents interaction between molecules when Bio50 undergoes N_2 thermochemical conversion.

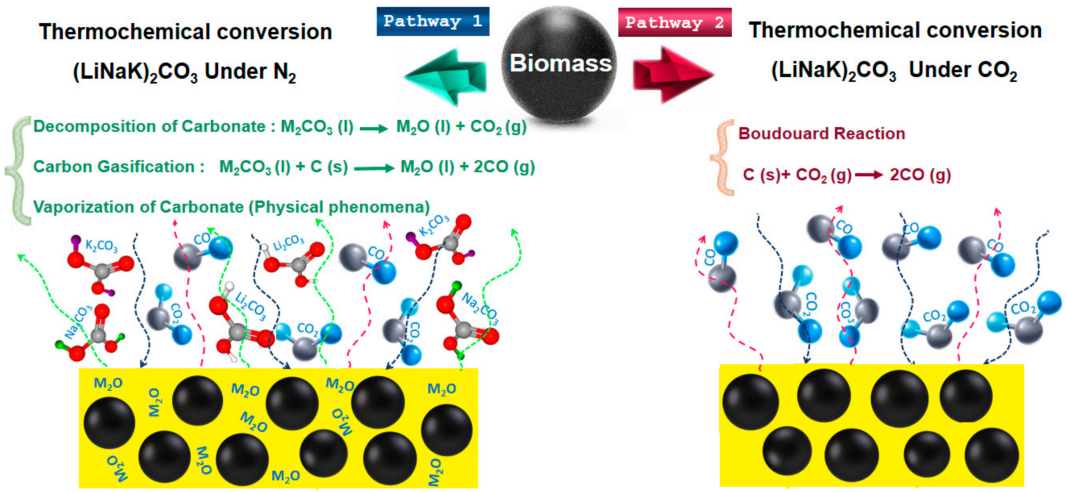

Figure 8. Graphical illustration of biomass thermochemical conversion in molten carbonate ($[LiNaK]_2(CO)_3$ under N_2 and CO_2 at 900 °C.

The complexity of various chemical reactions, such as carbon/carbonate gasification, molten carbonate decomposition, and physical phenomena, such as salt vaporization, registered a large mass loss in TGA (Figures 5 and 6). Above a temperature of 750 °C, all these reactions gradually took place, differentiating that each contribution was intricate. At first, because of a high amount of weight decrease in Bio50-N_2, it was that assumed carbon/carbonate gasification was the main pathway of carbonaceous fuel consumption and a higher amount of CO generation should be measured by GC (Figure 7). However, the extent of mass loss and the amount of generated CO_2 expressed molten

carbonate decomposition as the dominant route, which appeared to be accelerated in the presence of carbon particles. Other groups have also reported carbon/carbonate gasification and carbonate decomposition [34,44,57]. Kopyscincki's group [22] studied K_2CO_3 reaction with carbon particles from acid washed coal under N_2. According to their findings above 800 °C (close to K_2CO_3 melting point at 891 °C), cleavage of K and carbon complex supplied appropriate conditions for potassium vaporization from the surface of carbon. Since they applied acid-washed coal and a single solid salt, they assumed they generated CO as the dominant gas from carbon/K_2CO_3 gasification. In our work, because the ternary eutectic had a lower melting point (~400 °C) than potassium carbonate (891 °C), vaporization of salts at 900 °C was expected to be more important (which was frequently sighted during experiments (Figure S2)). Therefore, ternary carbonate decomposition and vaporization were dominant over carbon/carbonate gasification. Although most of the available researches are limited to single or binary carbonate gasification, Glenn et al. [39] inspected interaction between coal particles and ternary molten carbonate (Li_2CO_3, Na_2CO_3, and K_2CO_3 (43.5: 31.5: 25 mol.%, respectively)) up to 800 °C. The phenomena of coal/carbonate reaction under N_2 and CO_2 was in accordance with our outcome. Previously, in the absence of GC data, the suggested reaction mechanism was carbonate gasification under N_2, as well as enhancing the Boudouard reaction when the gaseous injected switched to CO_2 at 800 °C.

Overall, GC analysis of this work proves that carbon/carbonate is the weaker chemical interaction compared to decomposition and vaporization of liquid carbonate (ternary eutectic). However, to separate and measure the exact amount of salt vaporization (physical phenomena) from salt decomposition (chemical reaction) or any other possible pathway for further mass loss under inert environment, additional research into a highly equipped set up would be required.

The left pathway of Figure 8 demonstrates the Boudouard reaction, which is the dominant mechanism of mass loss at 900 °C under CO_2, where the gas consumes carbon particles in the presence of stable molten carbonate. Molten carbonate has no decomposition or vaporization under CO_2 [35] and is well known to accelerate the reverse Boudouard reaction [3,23,40,55,58]. The outcome of this work (Figures 5 and 6) also demonstrated improvement of CO_2 gasification onset temperature from ~735 °C in untreated biomass to ~640 °C for Bio50-CO_2, as the circumstance of the carbonate catalytic effect with additional possibility of carbonate gasification increased observed mass loss.

The beneficial output of this work gives better understanding of carbonate performance and properties in various atmospheres and temperatures, which is applicable in different technologies, apart from biomass thermochemical conversion, such as solar thermal plants, fuel cells, and the direct carbon fuel cell.

5. Conclusions

The interaction of biomass and carbonate ($[LiNaK]_2$ $(CO)_3$) was investigated under N_2 and CO_2 at two different temperatures (600 °C and 900 °C). Results from 600 °C demonstrated suppressing of raw biomass devolatilization in the presence of molten carbonate, regardless of carrier gas types, and showed a slight increase in mass loss observed for CO_2 atmospheres. The phenomena of swelling and bubble-shaped particles of remnant char from Bio50-CO_2 was observed, which are the results of less devolatilization compared with Bio-CO_2 (with 6 wt.% deviation in weight decrease) and a possible effect of carbonate in tar reduction. Experiments at a high temperature (900 °C) established the stability of carbonate under CO_2 and demonstrated a reduction in starting temperature for the onset of Boudoard gasification (~640 °C). However, under N_2, the system was exposed to complex concurrent chemical reactions and physical vaporization phenomena with a number of synergistic reaction pathways observed. In the presence of carbon particles, molten carbonate decomposed more and generated more than three times the amount of CO_2 in GC analysis compared to CO. This result demonstrates the dominant pathway of decomposition and vaporization under nitrogen in comparison with carbon/carbonate gasification.

Supplementary Materials: The following are available online at http://www.mdpi.com/1996-1073/13/20/5395/s1, Figure S1: SEM image of particle distribution and surface morphology from Bio50-N_2 water washed char at 600 °C, Figure S2: Vaporization of $LiNaK_2$ (CO_3) under N_2 at 900 °C inside TGA column. Covers crucible, hookers and other sections.

Author Contributions: Conceptualization, T.J. and J.A.; methodology, T.J. and J.A.; formal analysis, T.J. and J.A.; writing—original draft preparation, T.J.; writing—review and editing, J.A. and B.M.; supervision, J.A. and B.M. All authors have read and agreed to the published version of the manuscript.

Funding: This research received no external funding.

Conflicts of Interest: The authors declare no conflict of interest.

References

1. Basu, P. *Biomass Gasification, Pyrolysis and Torrefaction: Practical Design and Theory*; Elsevier Science: Amsterdam, The Netherlands, 2013.
2. Lahijani, P.; Mohammadi, M.; Zainal, Z.A.; Mohamed, A. Advances in CO_2 gasification reactivity of biomass char through utilization of radio frequency irradiation. *Energy* **2015**, *93*, 976–983. [CrossRef]
3. Lahijani, P.; Mohammadi, M. Catalytic Effect of Metal Species on Enhancement of CO_2 Gasification Reactivity of Biomass Char. *Int. J. Eng.* **2015**, *28*, 1251–1256.
4. Nunes, L.; Matias, J.; Catalão, J. Biomass combustion systems: A review on the physical and chemical properties of the ashes. *Renew. Sustain. Energy Rev.* **2016**, *53*, 235–242. [CrossRef]
5. Yuan, P.; Wang, J.; Pan, Y.; Shen, B.; Wu, C. Review of biochar for the management of contaminated soil: Preparation, application and prospect. *Sci. Total. Environ.* **2019**, *659*, 473–490. [CrossRef] [PubMed]
6. Chhiti, Y.; Ouladsine, R.; Sahibeddine, A.; Bensitel, M. Catalytic effect of ash on bio-oil thermal conversion. *Moroc. J. Chem.* **2016**, *4*, 584–591.
7. Jalalabadi, T.; Li, C.; Yi, H.; Lee, D. A TGA study of CO_2 gasification reaction of various types of coal and biomass. *J. Mech. Sci. Technol.* **2016**, *30*, 3275–3281. [CrossRef]
8. Wang, L.; Li, T.; Vaárhegyi, G.; Skreiberg, Ø.; Løvås, T. CO_2 Gasification of Chars Prepared by Fast and Slow Pyrolysis from Wood and Forest Residue: A Kinetic Study. *Energy Fuels* **2018**, *32*, 588–597. [CrossRef]
9. Russell, S.H.; Turrion-Gomez, J.L.; Meredith, W.; Langston, P.A.; Snape, C. Increased charcoal yield and production of lighter oils from the slow pyrolysis of biomass. *J. Anal. Appl. Pyrolysis* **2017**, *124*, 536–541. [CrossRef]
10. Azwar, E.; Mahari, W.A.W.; Chuah, J.H.; Vo, D.V.N.; Ma, N.L.; Lam, W.H.; Lam, S.S. Transformation of biomass into carbon nanofiber for supercapacitor application—A review. *Int. J. Hydrog. Energy* **2018**, *43*, 20811–20821. [CrossRef]
11. Chhiti, Y.; Kemiha, M. Thermal conversion of biomass, pyrolysis and gasification. *Int. J. Eng. Sci. (IJES)* **2013**, *2*, 75–85.
12. Belgaum, V. Tar formation, Reduction and Technology of Tar during Biomass Gasification/Pyrolysis—An Overview. *Int. J. Eng. Res. Technol.* **2017**, *6*. [CrossRef]
13. Sharma, R.K.; Wooten, J.B.; Baliga, V.L.; Lin, X.; Chan, W.G.; Hajaligol, M.R. Characterization of chars from pyrolysis of lignin. *Fuel* **2004**, *83*, 1469–1482. [CrossRef]
14. Menon, V.; Rao, M. Trends in bioconversion of lignocellulose: Biofuels, platform chemicals & biorefinery concept. *Prog. Energy Combust. Sci.* **2012**, *38*, 522–550. [CrossRef]
15. Masnadi, M.S.; Grace, J.R.; Bi, X.T.; Lim, C.J.; Ellis, N. From fossil fuels towards renewables: Inhibitory and catalytic effects on carbon thermochemical conversion during co-gasification of biomass with fossil fuels. *Appl. Energy* **2015**, *140*, 196–209. [CrossRef]
16. Gonzaález, J.F.; Romaán, S.; Gonzaález-GarciÍa, C.M.; Nabais, J.M.V.; Ortiz, A.L. Porosity Development in Activated Carbons Prepared from Walnut Shells by Carbon Dioxide or Steam Activation. *Ind. Eng. Chem. Res.* **2009**, *48*, 7474–7481. [CrossRef]
17. Dong, S.; He, X.; Zhang, H.; Xie, X.; Yu, M.; Yu, C.; Xiao, N.; Qiu, J. Surface modification of biomass-derived hard carbon by grafting porous carbon nanosheets for high-performance supercapacitors. *J. Mater. Chem. A* **2018**, *6*, 15954–15960. [CrossRef]
18. Luo, K.; Zhang, C.; Zhu, S.; Bai, Y.; Li, F. Tar formation during coal pyrolysis under N2 and CO_2 atmospheres at elevated pressures. *J. Anal. Appl. Pyrolysis* **2016**, *118*, 130–135. [CrossRef]

19. Jalalabadi, T.; Glenn, M.; Tremain, P.; Moghtaderi, B.; Donne, S.W.; Allen, J. Modification of Biochar Formation during Slow Pyrolysis in the Presence of Alkali Metal Carbonate Additives. *Energy Fuels* **2019**, *33*, 11235–11245. [CrossRef]
20. Umeki, K.; Häggström, G.; Bach-Oller, A.; Kirtania, K.; Furusjö, E. Reduction of Tar and Soot Formation from Entrained-Flow Gasification of Woody Biomass by Alkali Impregnation. *Energy Fuels* **2017**, *31*, 5104–5110. [CrossRef]
21. Hayashi, J.; Kazehaya, A.; Muroyama, K.; Watkinson, A. Preparation of activated carbon from lignin by chemical activation. *Carbon* **2000**, *38*, 1873–1878. [CrossRef]
22. Kopyscinski, J.; Rahman, M.; Gupta, R.; Mims, C.A.; Hill, J.M. K_2CO_3 catalyzed CO_2 gasification of ash-free coal. Interactions of the catalyst with carbon in N_2 and CO_2 atmosphere. *Fuel* **2014**, *117*, 1181–1189. [CrossRef]
23. Bach-Oller, A.; Fursujo, E.; Umeki, K. Effect of potassium impregnation on the emission of tar and soot from biomass gasification. *Energy Procedia* **2019**, *158*, 619–624. [CrossRef]
24. Trubetskaya, A.; Larsen, F.H.; Shchukarev, A.; Ståhl, K.; Umeki, K. Potassium and soot interaction in fast biomass pyrolysis at high temperatures. *Fuel* **2018**, *225*, 89–94. [CrossRef]
25. Guo, J.; Lua, A.C. Textural and chemical characterizations of adsorbent prepared from palm shell by potassium hydroxide impregnation at different stages. *J. Colloid Interface Sci.* **2002**, *254*, 227–233. [CrossRef]
26. Raymundo-Piñero, E.; Azaïs, P.; Cacciaguerra, T.; Cazorla-Amorós, D.; Linares-Solano, A.; Béguin, F. KOH and NaOH activation mechanisms of multiwalled carbon nanotubes with different structural organisation. *Carbon* **2005**, *43*, 786–795. [CrossRef]
27. Prauchner, M.J.; Sapag, K.; Rodríguez-Reinoso, F. Tailoring biomass-based activated carbon for CH_4 storage by combining chemical activation with H_3PO_4 or $ZnCl_2$ and physical activation with CO_2. *Carbon* **2016**, *110*, 138–147. [CrossRef]
28. Rutkowski, P. Pyrolysis of cellulose, xylan and lignin with the K_2CO_3 and $ZnCl_2$ addition for bio-oil production. *Fuel Process. Technol.* **2011**, *92*, 517–522. [CrossRef]
29. Senneca, O.; Cerciello, F.; Heuer, S.; Ammendola, P. Slow pyrolysis of walnut shells in nitrogen and carbon dioxide. *Fuel* **2018**, *225*, 419–425. [CrossRef]
30. Fu, P.; Yi, W.; Li, Z.; Bai, X.; Wang, L. Evolution of char structural features during fast pyrolysis of corn straw with solid heat carriers in a novel V-shaped down tube reactor. *Energy Convers. Manag.* **2017**, *149*, 570–578. [CrossRef]
31. Kim, Y.; Oh, J.I.; Vithanage, M.; Park, Y.K.; Lee, J.; Kwon, E.E.; Ok, J.I. Modification of biochar properties using CO_2. *Chem. Eng. J.* **2019**, *372*, 383–389. [CrossRef]
32. Kirtania, K.; Axelsson, J.; Matsakas, L.; Christakopoulos, P.; Umeki, K.; Furusjö, E. Kinetic study of catalytic gasification of wood char impregnated with different alkali salts. *Energy* **2017**, *118*, 1055–1065. [CrossRef]
33. Hathaway, B.J.; Davidson, J.H.; Kittelson, D.B. Solar Gasification of Biomass: Kinetics of Pyrolysis and Steam Gasification in Molten Salt. *J. Sol. Energy Eng.* **2011**, *133*, 021011. [CrossRef]
34. McKee, D.W. Catalytic effects of alkaline earth carbonates in the carbon-carbon dioxide reaction. *Fuel* **1980**, *59*, 308–314. [CrossRef]
35. Olivares, R.I.; Chen, C.; Wright, S. The Thermal Stability of Molten Lithium–Sodium–Potassium Carbonate and the Influence of Additives on the Melting Point. *J. Sol. Energy Eng.* **2012**, *134*, 041002. [CrossRef]
36. Glenn, M.J.; Allen, J.; Donne, S.W. Thermal Investigation of a Doped Alkali-Metal Carbonate Ternary Eutectic for Direct Carbon Fuel Cell Applications. *Energy Fuels* **2015**, *29*, 5423–5433. [CrossRef]
37. Glenn, M.; Mathan, B.; Islam, M.; Beyad, Y.; Allen, J.A.; Donne, S.W. Gas Atmosphere Effects Over the Anode Compartment of a Tubular Direct Carbon Fuel Cell Module. *Energy Fuels* **2019**, *33*, 7901–7907. [CrossRef]
38. Fereres, S.; Prieto, C.; Gavarrell, P.G.; Rodríguez, A.; Sánchez-Jiménez, P.E.; Pérez-Maqueda, L.A. Molten carbonate salts for advanced solar thermal energy power plants: Cover gas effect on fluid thermal stability. *Sol. Energy Mater. Sol. Cells* **2018**, *188*, 119–126. [CrossRef]
39. Glenn, M.J.; Allen, J.A.; Donne, S.W. Carbon Gasification from a Molten Carbonate Eutectic. *Energy Technol.* **2019**, *7*. [CrossRef]
40. Klopper, L.; Strydom, C.A.; Bunt, J.R. Influence of added potassium and sodium carbonates on CO_2 reactivity of the char from a demineralized inertinite rich bituminous coal. *J. Anal. Appl. Pyrolysis* **2012**, *96*, 188–195. [CrossRef]
41. Mallick, D.; Mahanta, P.; Moholkar, V.S. Co-gasification of coal and biomass blends: Chemistry and engineering. *Fuel* **2017**, *204*, 106–128. [CrossRef]

42. Hughes, M.A.; Allen, J.; Donne, S.W. The properties and performance of carbon produced through the electrochemical reduction of molten carbonate: A study based on step potential electrochemical spectroscopy. *Electrochim. Acta* **2018**, *278*, 340–351. [CrossRef]
43. Li, C.; Yi, H.; Jalalabadi, T.; Lee, D. Thermal decomposition of alkane hydrocarbons inside a porous Ni anode for fuel supply of direct carbon fuel cell: Effects of morphology and crystallinity of carbon. *J. Power Sources* **2015**, *294*, 284–291. [CrossRef]
44. Peng, F.; Li, Y.; Nash, P.; Cooper, J.F.; Parulekar, S.J.; Selman, J.R. Direct Carbon Fuel Cells—Wetting behavior of graphitic carbon in molten carbonate. *Int. J. Hydrog. Energy* **2016**, *41*, 18858–18871. [CrossRef]
45. Yoshida, S.; Matsunami, J.; Hosokawa, Y.; Yokota, O.; Tamaura, Y.; Kitamura, M. Coal/CO_2 Gasification System Using Molten Carbonate Salt for Solar/Fossil Energy Hybridization. *Energy Fuels* **1999**, *13*, 961–964. [CrossRef]
46. Yeboah, Y.D.; Xu, Y.; Sheth, A.; Godavarty, A.; Agrawal, P.K. Catalytic gasification of coal using eutectic salts: Identification of eutectics. *Carbon* **2003**, *41*, 203–214. [CrossRef]
47. Claes, P.; Moyaux, D.; Peeters, D. Solubility and solvation of carbon dioxide in the molten $Li_2CO_3/Na_2CO_3/K_2CO_3$ (43.5:31.5:25.0 mol-%) eutectic mixture at 973 K I. Experimental part. *Eur. J. Inorg. Chem.* **1999**, *1999*, 583–588. [CrossRef]
48. Jalalabadi, T.; Drewery, M.; Tremain, P.; Wilkinson, J.; Moghtaderi, B.; Allen, J. The Impact of Carbonate Salts on Char and Gaseous Evolution during Slow Pyrolysis of Biomass, Cellulose, and Lignin. *Sustain. Energy Fuels* **2020**. [CrossRef]
49. Nygård, H.S.; Olsen, E. Molten salt pyrolysis of milled beech wood using an electrostatic precipitator for oil collection. *AIMS Energy* **2015**, *3*, 284–296. [CrossRef]
50. Su, S.; Song, Y.; Wang, Y.; Li, T.; Hu, S.; Xiang, J.; Li, C.Z. Effects of CO_2 and heating rate on the characteristics of chars prepared in CO_2 and N_2 atmospheres. *Fuel* **2015**, *142*, 243–249. [CrossRef]
51. Khan, M.R.; Jenkins, R.G. Influence of Added Calcium Compounds on Swelling, Plastic, and Pyrolysis Behavior of Coal Devolatilized at Elevated Pressures. *Fuel* **1986**, *65*, 1203–1208. [CrossRef]
52. Khan, M.; Jenkins, R.G. Swelling and plastic properties of coal devolatilized at elevated pressures: An examination of the influences of coal type. *Fuel* **1986**, *65*, 725–731. [CrossRef]
53. Riaza, J.; Ajmi, M.; Gibbins, J.; Chalmers, H. Ignition and combustion of single particles of coal and biomass under O_2/CO_2 atmospheres. In Proceedings of the 13th International Conference on Greenhouse Gas Control Technologies, Ghgt-13, Lausanne, Switzerland, 14–18 November 2016; 2017; Volume 114, pp. 6067–6073.
54. Riaza, J.; Khatami, R.; Levendis, Y.A.; Álvarez, L.; Gil, M.V.; Pevida, C.; Rubiera, F.; Pis, J.J. Combustion of single biomass particles in air and in oxy-fuel conditions. *Biomass Bioenergy* **2014**, *64*, 162–174. [CrossRef]
55. Perander, M.; DeMartini, N.; Brink, A.; Kramb, J.; Karlström, O.; Hemming, J.; Moilanen, A.; Konttinen, J.; Hupa, M. Catalytic effect of Ca and K on CO_2 gasification of spruce wood char. *Fuel* **2015**, *150*, 464–472. [CrossRef]
56. Mims, C. *Catalytic Gasification of Carbon: Fundamentals and Mechanism, in Fundamental Issues in Control of Carbon Gasification Reactivity*; Springer: Berlin/Heidelberg, Germany, 1991; pp. 383–407.
57. McKee, D.; Chatterji, D. The catalytic behavior of alkali metal carbonates and oxides in graphite oxidation reactions. *Carbon* **1975**, *13*, 381–390. [CrossRef]
58. An, W.; Sun, X.; Jiao, Y.; Wang, S.; Wang, W.; Tadé, M.O.; Shao, Z.; Li, S.D.; Shuang, S. Inherently Catalyzed Boudouard Reaction of Bamboo Biochar for Solid Oxide Fuel Cells with Improved Performance. *Energy Fuels* **2018**, *32*, 4559–4568. [CrossRef]